How to cite: *Angew. Chem. Int. Ed.* **2024**, *63*, e202408441
doi.org/10.1002/anie.202408441

Mussel-Inspired Adhesives | Hot Paper

Redox-Triggered Debonding of Mussel-Inspired Pressure Sensitive Adhesives: Improving Efficiency Through Functional Design

Tilmann J. Neubert, Keven Walter, Carolin Schröter, Victoria Guglielmotti, Karsten Hinrichs, Stefan Reinicke, Andreas Taden, Kannan Balasubramanian, and Hans G. Börner**

Abstract: Debondable pressure-sensitive adhesives (PSAs) promise access to recyclability in microelectronics in the transition toward a circular economy. Two PSAs were synthesized from a tetravalent thiol star-polyester forming thiol-catechol-connectivities (TCC) with either the biorelated DiDopa-bisquinone (BY*Q) or the fossil-based bisquinone A (BQA). The PSAs enable debonding by oxidation of TCC-catechols to quinones. The extent of debonding efficiency depends on the interaction modes, which are determined by the chemical structure differences of both TCC-motifs. BY*Q-TCC-PSA debonds with exceptional loss of 99 % of its approx. 2 MPa shear strength in glass-on-glass junctions. For BQA-TCC-PSA, a debonding efficiency of only approx. 60 % was found, irrespective of its initial shear strength, which could be tuned up to approx. 7 MPa. The efficiency of debonding for BY*Q-TCC-PSA after TCC-oxidation is linked to the loss of synergistic interactions without strongly affecting the bulk glue properties, outperforming the purely catechol-based BQA-analogue.

Biomimetic polymers often successfully focus only on the key features of their natural blueprints, reducing the complexity and cost of synthesis.[1] However, biorelated building blocks with complex sets of functionalities, might provide opportunities for deliberate design of efficient functional systems, which would otherwise go unnoticed by simplification.[2] In light of recent legislative demands[3] materials chemistry is challenged to foster the transformation toward circular economy with sustainable resources and smart repair/recycling strategies. Therein, debondable adhesives are considered as one of the key enabling platforms, e.g. for integrated electronic devices, reducing waste streams and the associated carbon footprint.[4] Such glues are deactivatable on demand by appropriate triggers, including heat, chemicals and others.[5] In polymer adhesives, the interactions of chemical motifs integrated into the network structure promote bulk cohesion and interfacial glue-substrate adhesion. Debonding-on-demand requires the deliberate implementation of stimulus-deactivatable interactions.

Recently, the thiol-quinone polyaddition route was introduced as a platform for mussel-inspired adhesive polymers, exhibiting thiol-catechol-connectivities (TCCs, Figure 1a) showing strong adhesive interactions on various substrate materials, even under water.[1a,b,6] Biogenic TCC-structures abstract cysteinyldopa-linkages containing L-3,4-dihydroxyphenylalanine (Dopa, Y*) as potent catechol interaction motifs.[7] Such catechols experience significant deterioration in adhesive properties upon oxidation to quinones, as pioneered for Dopa-bearing peptides by Messersmith *et al.*[8] and further developed by Waite *et al.*[9] and Lee *et al.*[10]

[*] Dr. T. J. Neubert, K. Walter, C. Schröter, V. Guglielmotti, Prof. Dr. K. Balasubramanian, Prof. Dr. H. G. Börner
Department of chemistry
Humboldt-Universität zu Berlin
Unter den Linden 6, 10117 Berlin, Germany
E-mail: nano.anchem@hu-berlin.de
h.boerner@hu-berlin.de

Dr. T. J. Neubert, Prof. Dr. K. Balasubramanian
School of Analytical Sciences Adlershof (SALSA) & IRIS Adlershof
Humboldt-Universität zu Berlin
Unter den Linden 6, 10117 Berlin, Germany

V. Guglielmotti
Instituto de Nanosistemas
Universidad Nacional de General San Martín
Av. 25 de Mayo 1021, San Martín, Provincia de Buenos Aires, Argentina

PD Dr. K. Hinrichs
Application Labs Berlin
Leibniz-Institut für Analytische Wissenschaften - ISAS - e.V.
Schwarzschildstraße 8, 12489 Berlin, Germany

PD Dr. K. Hinrichs
Nanoscale Solid-Liquid Interfaces
Helmholtz-Zentrum Berlin für Materialien und Energie GmbH
Schwarzschildstraße 8, 12489 Berlin, Germany

Dr. S. Reinicke
Life Science & Bioprocesses
Fraunhofer Institute for Applied Polymer Research IAP
Geiselbergstraße 69, 14476 Potsdam-Golm, Germany

Dr. A. Taden
Adhesive Research
Henkel AG & Co. KGaA
Henkelstraße 67, 40589 Düsseldorf, Germany

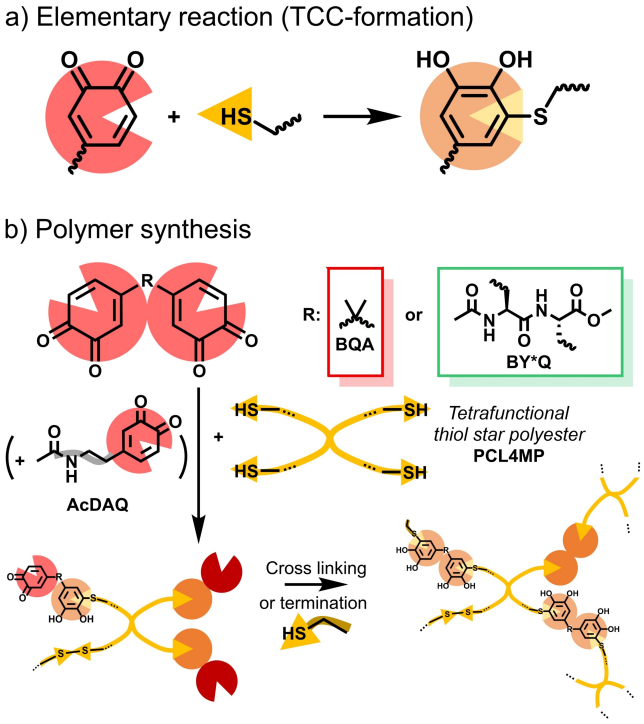

Figure 1. **Idealized synthesis pathways to TCC-PSAs.** a) Thiol-quinone Michael addition to form TCCs. b) TCC-polymer synthesis by reacting a thiol star polyester with BQA or BY*Q (+AcDAQ) including ethanethiol-quenching of terminal quinones.

Here, we introduce TCC-adhesives that exhibit permanent tack in the applicable state, representing debondable pressure-sensitive adhesives (TCC-PSA). Catechol-bearing PSAs have been demonstrated before.[11] However, here the TCC-polyaddition route was used to access modular adhesive polymers with tunable properties aiming at a combination of high tack and shear strength. Two TCC-PSAs were compared containing different TCC-entities, either the dipeptide-based DiDopa-bisquinone (BY*Q) or bisquinone A (BQA).[1a,b] A chemically triggered adhesion deactivation mechanism was revealed by correlating the selective chemical oxidation of the TCCs with nanoscopic and macroscopic changes in their adhesive properties.

To synthesize TCC-PSAs, the tetrafunctional thiol star polyester, polycaprolactone-tetra-(3-mercaptopropionate) (PCL4MP, Figure S1 & S7 in Supporting Information - SI) was applied as low-T_g building block to react with BY*Q or BQA (Figure 1). BY*Q can be sourced from amino acids, while BQA is derived from the fossil-based bisphenol A (BPA). BY*Q-TCC-polymers offer multiple interactions among the peptidic TCC-entities, including interpolymeric catechol-catechol and catechol-amide H-bonding, as well as peptidic interactions.[12] Of these, BQA-TCC-polymers only share catechol-catechol interactions, as their backbone is comparatively simple (Figure 1b). Considering the different interaction patterns present in these TCC-polymers, diverging debonding efficiencies might be anticipated upon TCC-catechol oxidation.

For the TCC-PSAs, different thiol:quinone-ratios (T:Q-ratio) were screened (*cf.* Figure 2 and SI-Section 2). By adjusting the T:Q-ratio, the molecular weight distribution changes from small unimers to large networks. A broader distribution is associated with a stronger adhesive, as higher molecular weight fractions promote cohesion and toughness through stronger networks, while lower molecular weight fractions enhance wetting and spreading. Finger tack tests can be used to obtain a first impression on tackiness (Figure S9). The optimal T:Q-ratios for the TCC-PSAs were determined based on applicability and performance. Strong adhesive properties and broad molecular weight distributions were targeted, balancing viscoelasticity, tack and cohesion, while maintaining solubility. For BQA, the T:Q-ratio could be adjusted down to 1:1.2, increasing $M_{w,app}$ to 140 kg/mol with $Đ = 9.9$ and establishing a high molecular weight flank of up to 2×10^6 g/mol (Figure 2a), yielding the ductile and tacky **BQA-TCC-PSA** with a T_g of +9°C. For BY*Q, the optimization was more challenging, as BY*Q synthesis required DiDopa-activation in solution with sodium periodate ($NaIO_4$). This facilitated competitive disulfide formation during the polyaddition. Moreover, the pronounced self-interactions of peptides in BY*Q-TCC-polymers led to non-tacky, brittle materials (Figure S9). To broaden dispersity, while avoiding covalent crosslinking, the bivalent BY*Q was partially replaced by monovalent *N*-acetyl dopamine-quinone (AcDAQ), implementing non-bridging TCC-motifs. The highly tacky, viscoelastic **BY*Q-TCC-PSA** with a T_g of -27°C was finally isolated with a T:Q-ratio of 1:1.5 at a bisquinone:monoquinone-ratio (BQ:MQ-ratio) of 1:3. GPC revealed $M_{w,app} = 47$ kg/mol with $Đ = 12.8$ and a high molecular weight fraction reaching 10^6 g/mol (Figure 2b).

^{1}H-NMR spectroscopy of purified TCC-PSAs confirmed their chemical structures, containing PCL4MP cores and aromatic TCC-functionalities (Figure S14-S15). Thereby, a molecular ratio of PCL4MP to BQA of 1:2.2 was estimated for BQA-TCC-PSA. Due to the intricate nature of the BY*Q-TCC-PSA network, NMR spectroscopy allowed only a rough estimation of the ratios between PCL4MP, BY*Q-TCC and AcDAQ-TCC to be 1:0.9:1.2, suggesting disulfides as a pronounced network-forming motif (SI-Section 2.4-5).

For efficient oxidative debonding of the TCC-PSAs, the chemical trigger ($NaIO_4$) requires access to the gluing interface. Previously, Ravoo *et al.* demonstrated patterned application of polymer-brush-adhesives e.g. with catechol-boronate-interactions.[13] Both TCC-PSAs were compatible with microcontact printing onto glass via micropatterned polydimethylsiloxane (PDMS) stamps to print separated bondlines with 5 µm width (Figure S19). AFM in quantitative imaging (QI) mode in air and water served as a tool for analytical characterization of TCC-PSAs with minimal material requirements (Figure 3, Figure S22). The QI-mode can be described as a nano-tack experiment,[14] probing interfacial interactions and reading multiple properties like topography, Young's modulus (YM) and adhesive parameters with sub-micron resolution, yielding statistically reliable values (Figure S20-S21). Measurements on micropatterned

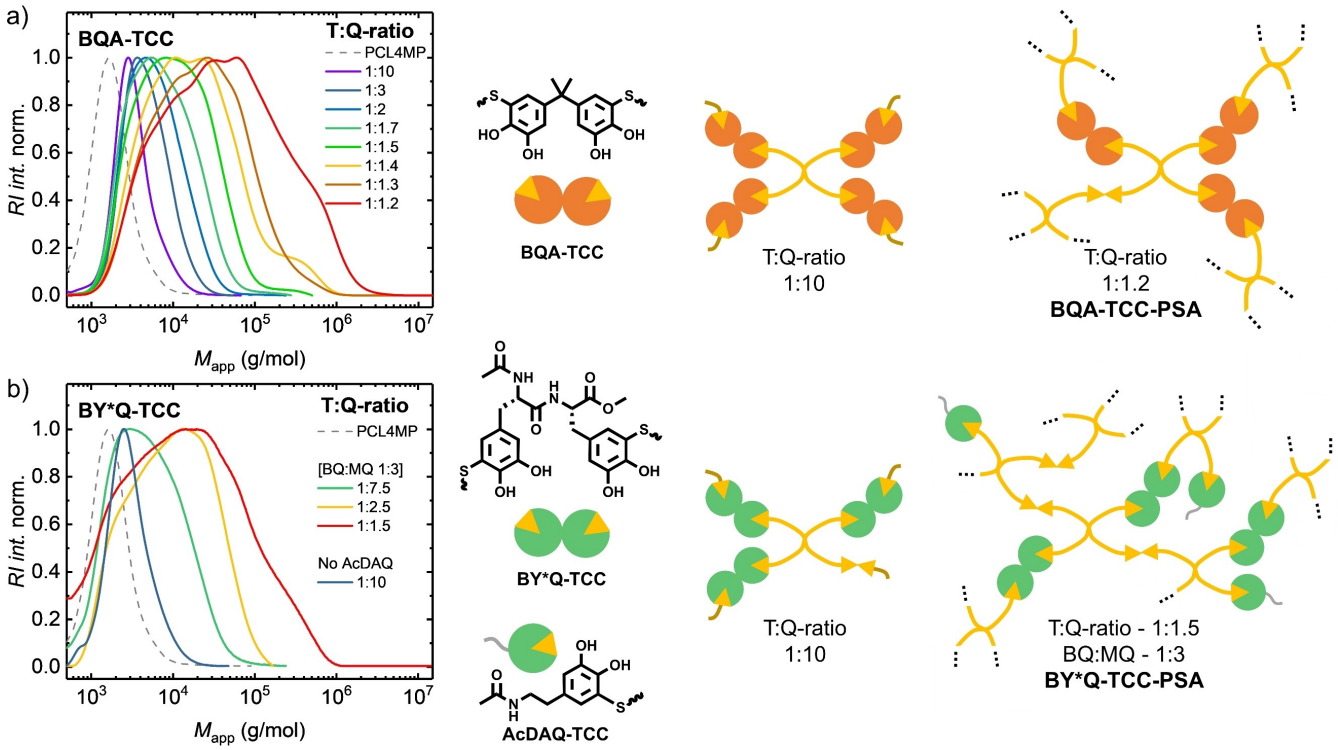

Figure 2. **Product analysis by gel permeation chromatography (GPC, left) and schematic illustration of network structures corresponding to the indicated ratios (right).** The molecular weight distribution of TCC-polymers shows a dependence on the used thiol:quinone-ratio (T:Q-ratio) of the monomers PCL4MP and a) BQA or b) BY*Q (*cf.* Table S1 for extracted values).

substrates resulted in high material contrast, where uncoated regions act as internal references.

In Figure 3, BY*Q-TCC-PSA formed vaulted stripes of 400 ± 90 nm height on the substrate. BQA-TCC-PSA transferred less smooth and led to rather uneven lines of 160 ± 140 nm thickness. Viscoelasticity is a key property of PSAs that greatly contributes to their adhesive profile, but also defines applicability.[15] With 1.8 ± 0.3 MPa, the YM of BY*Q-TCC-PSA was much lower than that of BQA-TCC-PSA (10.3 ± 4.6 GPa), explaining the smoother printing of BY*Q-TCC-PSA. Both PSAs showed similar adhesion of ~100 nN, but differ strongly in work of adhesion (WoA, Table S2, Figure S24). The softer BY*Q-TCC-PSA exhibited a high WoA-profile (~30 fJ) associated with PSA-characteristic fibrillation.[16] BQA-TCC-PSA reached WoA <1 fJ and showed less tack than BY*Q-TCC-PSA. Overall, the nano-tack tests confirmed that both TCC-PSAs present interfacial adhesion, but BQA-TCC-PSA is less elastic than BY*Q-TCC, while the latter shows more tack. In direct comparison to commercial variants, only BY*Q-TCC-PSA follows the typical guidelines for properties of PSAs with its low YM and T_g, and a characteristic force-distance-curve (Figure S24a). However, BQA-TCC-PSA still presents a tacky surface and can be tuned further towards PSA characteristics by adjusting the T:Q-ratio (Figure S24b,c).

Furthermore, the AFM-QI measurements made it possible to directly observe the oxidation effect (Figure 3b-c). The adhesive properties of both TCC-PSAs deteriorated after incubation with $NaIO_4$-solution, supposedly due to the oxidation of TCC-catechols to quinones.[6a] The WoA was reduced by approx. two thirds for both TCC-PSAs in air (Table S2, Figure S24). Under water, the WoA decreased by ~93% for BY*Q-TCC and ~45% for BQA-TCC. The YM of both TCC-PSAs, but especially that of BY*Q-TCC-PSA, increased slightly in the dry state after oxidation, suggesting changes in the cohesive network interactions caused by oxidation of the TCC-functionalities (Table S3). Overall, the measurements confirmed the importance of TCC-redox states for adhesive properties by indicating a loss of tackiness, which was consistent with previous measurements of Dopa-derivatives.[8,9b]

The commonly used strong oxidant $NaIO_4$ ensures high reaction rates, whereby crosslinking between quinones with catechols along the well-described mechanism of Dopa-dimerization is effectively suppressed.[17] Aging through autooxidation by oxygen was not diminishing the adhesive properties of bondlines stored for eight months in air, justifying the need for a strong chemical trigger (*cf.* SI-Section 5.4). Weaker oxidants such as H_2O_2 or $NaIO_3$ did not have the desired effect. The application of basic pH conditions, using solutions of either NaOH or the electrochemically accessible "green" periodate-alternative para-periodate[18] ($Na_3IO_4(OH)_2$) resulted in severe side reactions and caused the PSA-films to turn black, immediately (*cf.* SI-Section 4.5). Instead, incubation of both TCC-PSAs with acidic meta-periodate ($NaIO_4$) resulted in the characteristic color changes, turning deeply orange/red (Figure S25, Videos "V1 BYQ-TCC oxidation", "V2 BQA-TCC oxida-

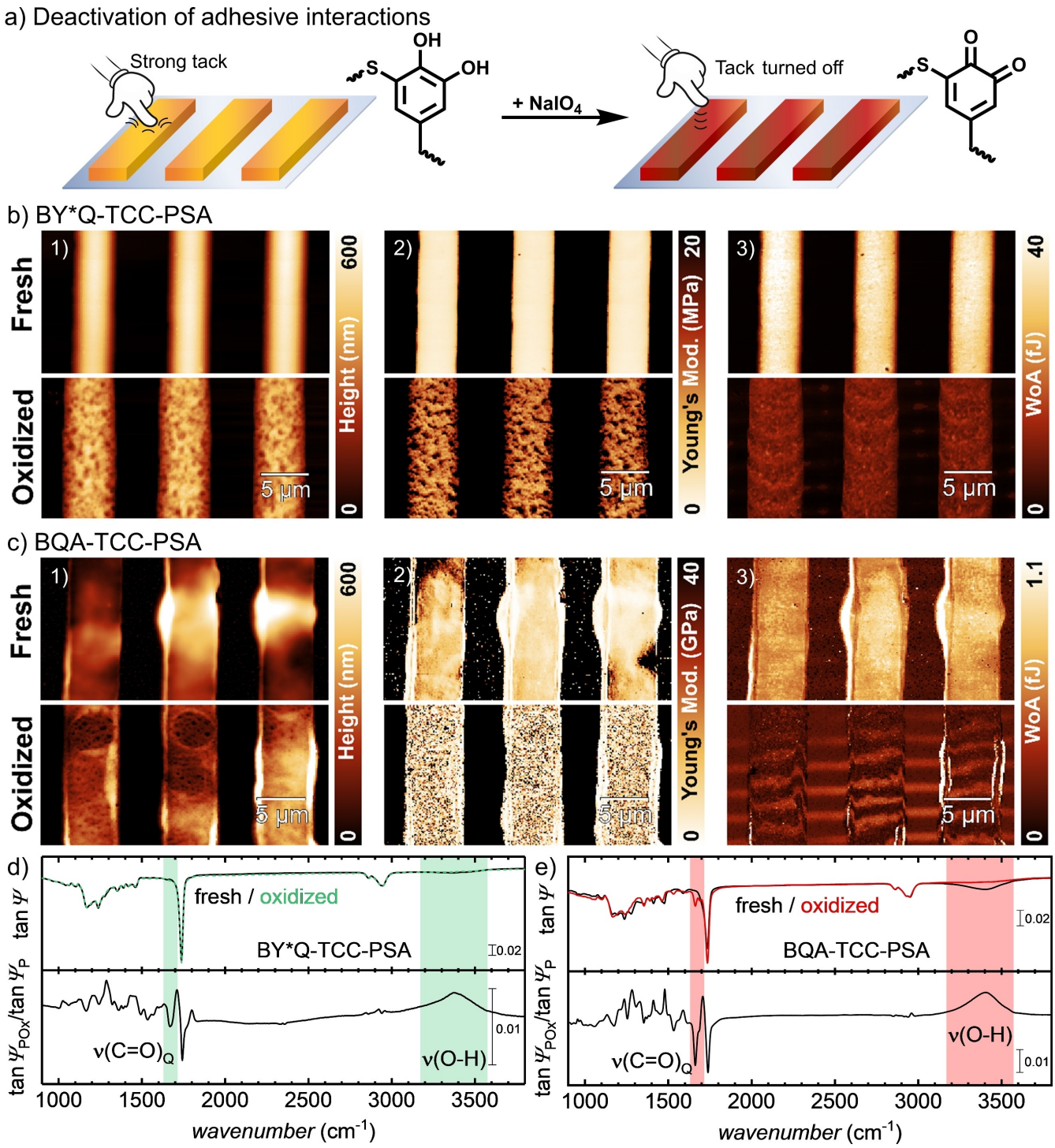

Figure 3. **Deactivation of tack in TCC-PSAs through chemical oxidation.** a) Schematic illustration of chemically triggered debonding in TCC-PSAs. b,c) AFM-QI maps comparing stripes of TCC-PSAs on glass prior to (upper half) and after oxidation (lower half). Extracted parameters: 1) topography, 2) Young's modulus (YM), and 3) work of adhesion (WoA). d,e) TanΨ-spectra of infrared-spectroscopic ellipsometry (IRSE) measurements of TCC-PSA films prior to (black, P) and after oxidation (green/red, POx) with ratioed spectrum (bottom). (Conditions: $NaIO_4$ (100 mM), 15 min; YM scale is adjusted for contrast).

tion"). This was verified by UV-Vis spectroscopy, which showed the quinone-characteristic absorption at ~370 nm.[1a] Thin-film sensitive infrared-spectroscopic ellipsometry (IRSE)[19] measurements confirmed the chemical transformation of the TCC-moieties. The broad catechol ν(OH)-vibration ~3400 cm^{-1} vanished upon oxidation, while a new quinone-characteristic ν(C=O)-band arose at 1670 cm^{-1} (Figure 3d-e).[20] The disappearance of the catechol ν(OH)-

vibration suggests full catechol oxidation in the film. Time-dependent UV-Vis measurements further support this observation (Figure S26). IRSE and XPS measurements suggested no severe additional chemical transformations (Figure 3, Figure S27). In addition, GPC of the redissolved oxidized polymer indicated no decomposition or crosslinking of the TCC-PSAs, justifying the use of the strong oxidant $NaIO_4$ (Figure S28). The catechol-/quinone-band intensities in the IRSE spectra were weaker for BY*Q-TCC-PSA than for BQA-TCC-PSA (Figure 3d-e, relative to PCL4MP signals, Figure S10). This aligns well with the lower fraction of TCCs in the network due to disulfide-bridges (SI-Section 2.4-5).

The nano-tack tests revealed impaired adhesive properties of the TCC-PSAs after oxidation, indicating the potential for macroscopic debonding. This was investigated using lap shear tests. Nano-tack and lap shear tests probe different aspects of adhesives (tack vs shear strength). However, predictions can be drawn from the earlier to the latter. For instance, BY*Q-TCC-PSA is softer and should withstand less load than BQA-TCC-PSA, while both should be weakened by oxidation. Note that a direct correlation of extracted values from both analyses is not straightforward due to differences probed in these tests, such as timescale, area of interaction, and direction of applied forces.

For lap shear tests, both TCC-PSAs were patterned in 200 µm wide bondlines by contact printing forming adhesive junctions with open channels (Figure S33). Larger and thicker bondlines were required for shear testing in comparison to nano-tack tests to form strong junctions with adequate adhesive wetting on both substrates. The channels allow for the oxidant to penetrate sufficiently into the adhesive layer for testing with and without oxidation revealing the debonding effect (Figure 4, Figure S35). Glass was chosen as the substrate, since it exhibited the highest shear strength among various substrate materials in pre-tests with BQA-TCC-PSA (Figure S34). Furthermore, glass is advantageous due to being transparent and chemically inert against the oxidant. Debonding of glass is especially interesting, as weakening of the glue interface prior to disassembly can prevent dangerous glass breakage.

Remarkably, upon oxidation the BY*Q-TCC-PSA revealed a virtually complete breakdown of the initial 2.0 MPa shear strength ($\tau_{Joint,}$ median, Figure 4). While some samples failed under their own weight during the oxidation, others could be tested and failed at remarkably small shear forces (Figure S35). BQA-TCC-PSA showed higher initial performance with $\tau_{Joint(med)}$ = 7.2 MPa, which declined to 3.4 MPa after oxidation. Both untreated TCC-PSAs failed cohesively, indicating strong glass adhesion. Upon oxidation, the glue-substrate interfaces were weakened, leading to adhesive failure, where the PSAs peeled-off cleanly from the glass (Figure 4d-e). Especially for ease of recyclability of the substrates it is noteworthy that the residues of BY*Q-TCC-PSA could be simply wiped off the glass immediately after oxidation.

In general, the performance of PSAs results from a complex interplay of several material parameters, defining the dynamics in the bulk and at the adhesive interface.

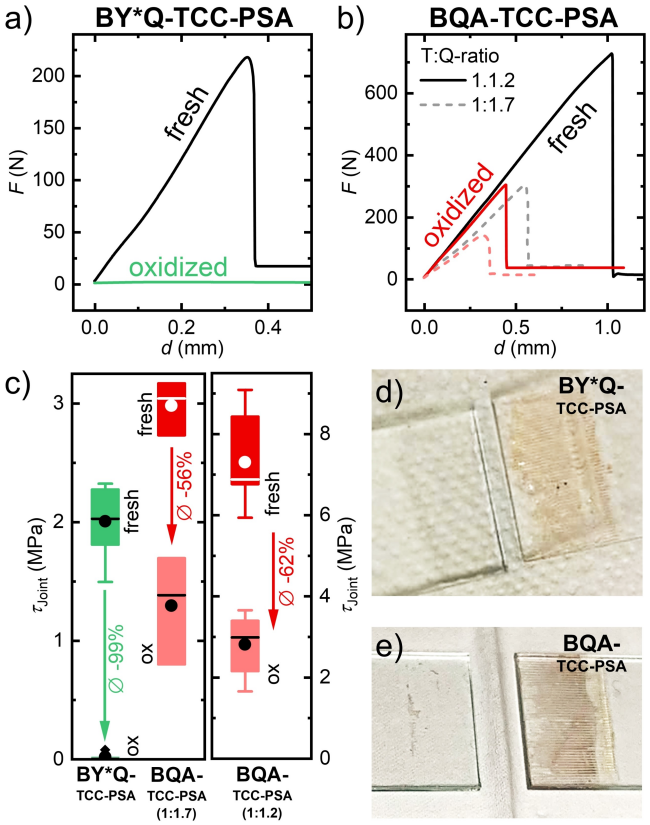

Figure 4. **Macroscopic debonding tests.** a,b) Shear tests performed on glass bonded by a) BY*Q-TCC-PSA and b) BQA-TCC-PSA (T:Q-ratio as indicated) applied in line patterns (200µm). c) Box plots of the joint strength (τ_{Joint}) of bonded substrates with untreated and oxidized TCC-PSA bondlines. d,e) Pictures of the failed junction on oxidized d) BY*Q-TCC-PSA and e) BQA-TCC-PSA (1:1.2).

However, despite this complexity, BY*Q-TCC-PSA could be crafted carefully to achieve respectable joint strengths and strong tack similar to typical PSAs.[15] In contrast to this, BQA-TCC-PSA exhibited higher YM and T_g, broader molecular weight distribution, and higher content of bivalent TCC-crosslinks, all of which promote and rationalize the considerably higher shear strength. It has been found for monodisperse model systems that catechols accompanied with amides can reach enhanced adhesion e.g. on glass, beyond values of isolated catechols.[12a] Taking this into account, the smaller fraction of TCC-entities present in BY*Q-TCC-PSA might be counterbalanced by additional interactions that originate from the peptide backbone.

The chemical oxidation of BQA-TCC-PSA caused a substantial decrease of τ_{Joint} by 62% on average. Under the same conditions, BY*Q-TCC-PSA exhibited a 99% reduction in shear strength, proving even higher suitability for effective debonding. The considerably lower initial shear strength of BY*Q-TCC-PSA compared to that of BQA-TCC-PSA was excluded as a potential reason for the effective debonding capability. A control experiment was conducted, using a softer BQA-TCC-PSA with a T:Q-ratio of 1:1.7 (*cf.* SI-Section 7). This PSA achieved $\tau_{Joint(med)}$ = 3.0 MPa and was only downregulated by 56% upon oxidation,

as well (Figure 4). Hence, the differences in the debonding efficiencies appear to originate from the structural and compositional differences between the BQA- and BY*Q-TCC-segments, which both undergo TCC-oxidation from catechols to quinones. Furthermore, GPC analysis of the oxidized adhesives showed no obvious crosslinking, which is in agreement with the use of the oxidant in excess (*cf.* SI-Section 4).[17b,c] Therefore, crosslinking could be excluded as another potential explanation for the superior debonding efficiency of BY*Q-TCC-PSA.

Nevertheless, the complete loss in adhesion of BY*Q-TCC-PSA remains a remarkable feature. Considering the underlying chemistry, the oxidation of BY*Q-TCC-catechols is expected to *i.*) strongly decrease enhanced catechol-substrate-adhesion,[12a] *ii.*) alter network cohesion by replacing catechol-catechol and catechol-amide H-bonding, while *iii.*) preserving the rather polar character of the TCC-connectivities due to the nature of the peptidic backbone. Hence, the chemical debonding is caused by distinct changes of the relevant catechol-interaction motif. The mechanism is supported by the observed changes from cohesive fracture before oxidation to adhesive failure after oxidation that occurred for both TCC-PSAs, suggesting a strong change at the adhesive interfaces. Furthermore, a slightly increased YM after oxidation, revealed that the bulk polymer network was not destabilized (Figure 3). This suggests that lost cohesive interactions might be compensated by quinone-amide H-bonding or hydrophobic interactions of the quinones.

In contrast, the oxidation of BQA-TCC-PSA has a considerably smaller effect on shear strength reduction. To understand this, the differences between the oxidized BQA-TCCs and BY*Q-TCCs segments have to be elucidated. Upon oxidation, the BQA-TCC-functionalities undergo a more pronounced change in properties, transforming from polar catechols to more hydrophobic quinonic structures (biscatechol A is water soluble, bisquinone A is not). This changes the interaction mode of the BQA-TCC-segments, which apparently partially compensates for loss of catechol adhesive interactions with increased hydrophobic interactions at the substrate interface and in the network. Comparable hydrophobic effects are expected to be much less pronounced in BY*Q-TCC-PSA, since the polarity of the network is preserved through the peptide-backbone structures and the BY*Q-TCC-entities constitute a smaller fraction of their respective polymer network. Apparently, the cohesive strength in the BQA-TCC-PSA bulk was not altered strongly, as neither the YM nor the shear stiffness changed dramatically upon oxidation (Table S3).

Overall, patterned TCC-polymers offer a platform for debondable PSAs. In practical examples, which favored the strength of the respective TCC-PSA, chemically triggered debonding was demonstrated for constantly stressed junctions (V3 BQA-TCC Weight stress test; V4 BYQ-TCC Weight stress test). Depending on the initial shear strength and debonding efficiency, these experiments were designed with tailored loads reaching from 50 g to 1 kg (*cf.* SI-Section 6).

In conclusion, a direct correlation between the redox state of TCC-catechols/quinones and the adhesive properties of TCC-PSA-polymers was revealed. Distinct debonding behaviors were observed for PSAs containing the peptidic DiDopa-bisquinone (BY*Q) *versus* the less functional bisquinone A (BQA). Depending on the network design, the shear strength of the polymers varies ranging from approx. 2 to 7 MPa on average. For both TCC-PSAs, the oxidation of the TCC-catechols resulted in a deterioration of adhesive properties as confirmed by independent nanoscopic and macroscopic experiments. Remarkably, the peptidic backbone of BY*Q-TCC-PSA offers synergistic interactions with the TCC-groups, the loss of which down-regulates shear strength by 99% after oxidation. In contrast, the oxidation of the BQA-TCC-PSAs reduces bond strength by approx. 60% as oxidation results in hydrophobic TCC-quinones that compensate the loss of cohesive and adhesive H-bond interactions through hydrophobic contacts. Advanced glue formulation strategies are expected to further improve the material performance. The oxidative trigger leaves room for further improvement, such as direct electrochemical debonding to avoid the need for strong chemical oxidants like sodium periodate paving the way towards end-consumer applications. Thus, the use of biorelated compounds offers opportunities to implement enhanced functionality into materials, broadening the design space for adhesive technologies as shown by TCC-adhesives that combine adhesive strength with efficient debonding.

Supporting Information

Experimental details, list of used chemicals & materials, synthesis and characterization of monomers and polymers, methodic details and additional data for AFM-QI, sample preparation AFM-QI and shear tests, shear test statistics, characterization of the polymers: NMR, UV-Vis, XPS, GPC.

The authors have cited additional references within the Supporting Information.[21-39]

Acknowledgements

TJN, KW, SR, AT and HGB acknowledge funding by German Federal Ministry of Education and Research BMBF (IBZT-01 031B1117A). TJN appreciates funding by the School for Analytical Sciences Adlershof (SALSA STF23-08). HGB acknowledges funding by the German Research Foundation (DFG) via project no. BO 1762/9-2 and KB via INST 276/754-1 (417915721). KH is grateful for the financial support by the Europäischer Fonds für regionale Entwicklung (EFRE) (1.8/13); the Ministerium für Innovation, Wissenschaft und Forschung des Landes Nordrhein-Westfalen; Senatsverwaltung für Wissenschaft, Gesundheit und Pflege des Landes Berlin and the BMBF. We thank A. Voelkel (MPIKGF) for providing DSC measurements and F. S. Zimmer for help with UV-Vis measurements. Open Access funding enabled and organized by Projekt DEAL.

Conflict of Interest

The authors declare no conflict of interest.

Keywords: debonding · green PSA · redox trigger · mussel-inspired adhesive · renewable building blocks

[1] a) J. M. Krüger, H. G. Börner, *Angew. Chem. Int. Ed.* **2021**, *60*, 6408–6413; b) J. M. Krüger, C.-Y. Choi, F. Lossada, P. Wang, O. Löschke, D. Auhl, H. G. Börner, *Macromolecules* **2022**, *55*, 989–1002; c) C. K. Chu, A. J. Joseph, M. D. Limjoco, J. Yang, S. Bose, L. S. Thapa, R. Langer, D. G. Anderson, *J. Am. Chem. Soc.* **2020**, *142*, 19715–19721; d) Y. Dou, Z.-P. Wang, W. He, T. Jia, Z. Liu, P. Sun, K. Wen, E. Gao, X. Zhou, X. Hu, J. Li, S. Fang, D. Qian, Z. Liu, *Nat. Commun.* **2019**, *10*, 5293; e) W. He, D. Qian, Y. Wang, G. Zhang, Y. Cheng, X. Hu, K. Wen, M. Wang, Z. Liu, X. Zhou, M. Zhu, *Adv. Mater.* **2022**, *34*, 2201843; f) J. Lee, C. Majidi, B. Schubert, R. S. Fearing, *J. R. Soc. Interface* **2008**, *5*, 835–844; g) H. Chung, R. H. Grubbs, *Macromolecules* **2012**, *45*, 9666–9673; h) Z. Ruan, S. Li, A. Grigoropoulos, H. Amiri, S. L. Hilburg, H. Chen, I. Jayapurna, T. Jiang, Z. Gu, A. Alexander-Katz, C. Bustamante, H. Huang, T. Xu, *Nature* **2023**, *615*, 251–258.

[2] a) G. Schmidt, K. H. Smith, L. J. Miles, C. K. Gettelfinger, J. A. Hawthorne, E. C. Fruzyna, J. J. Wilker, *Adv. Sci.* **2022**, *6*, 2100392; b) C. R. Westerman, B. C. McGill, J. J. Wilker, *Nature* **2023**, *621*, 306–311.

[3] a) https://eur-lex.europa.eu/resource.html?uri=cellar:b828d165-1c22-11ea-8c1f-01aa75ed71a1.0002.02/DOC 1&format=PDF; b) O. V. Mikichurova, I. V. Vlialko, *IOP Conf. Ser.: Earth Environ. Sci.* **2021**, *915*, 012022.

[4] a) X. Li, H. Liu, J. You, H. Diao, L. Zhao, W. Wang, *Waste Manag.* **2022**, *137*, 312–318; b) J. S. Lee, M. Kim, M. W. Lee, *Compos. Struct.* **2022**, *286*, 115290; c) S. Kirchhecker, A. Dell′Acqua, A. Angenvoort, A. Spannenberg, K. Ito, S. Tin, A. Taden, J. G. de Vries, *Green Chem.* **2021**, *23*, 957–965; d) I. McCulloch, M. Chabinyc, C. Brabec, C. B. Nielsen, S. E. Watkins, *Nat. Mater.* **2023**, *22*, 1304–1310.

[5] a) M. D. Banea, in *Structural Adhesive Joints*, **2020**, pp. 135–158; b) M. D. Banea, in *Progress in Adhesion and Adhesives*, **2020**, pp. 33–50; c) N. D. Blelloch, H. J. Yarbrough, K. A. Mirica, *Chem. Sci.* **2021**, *12*, 15183–15205; d) D. V. Srinivasan, S. Idapalapati, *Sustain. Mater. Technol.* **2021**, *30*, e00345; e) Z. Liu, F. Yan, *Adv. Sci.* **2022**, *9*, 2200264; f) K. R. Mulcahy, A. F. R. Kilpatrick, G. D. J. Harper, A. Walton, A. P. Abbott, *Green Chem.* **2022**, *24*, 36–61.

[6] a) J. Yang, M. A. Cohen Stuart, M. Kamperman, *Chem. Soc. Rev.* **2014**, *43*, 8271–8298; b) J. Horsch, P. Wilke, H. Stephanowitz, E. Krause, H. G. Börner, *ACS Macro Lett.* **2019**, *8*, 724–729; c) S. Arias, S. Amini, J. Horsch, M. Pretzler, A. Rompel, I. Melnyk, D. Sychev, A. Fery, H. G. Börner, *Angew. Chem. Int. Ed.* **2020**, *59*, 18495–18499; d) J. M. Kohn, J. Riedel, J. Horsch, H. Stephanowitz, H. G. Börner, *Macromol. Rapid Commun.* **2020**, *41*, 1900431; e) C.-Y. Choi, F. Lossada, K. Walter, T. Fleck-Kunde, S. Behrens, T. Meinelt, J. Falkenhagen, M. Hiller, H. Oschkinat, A. Dallmann, A. Taden, H. G. Börner, *Green Chem.* **2024**, *26*, 2044–2058; f) C. M. Schröter, L. D. Bangert, H. G. Börner, *ACS Macro Lett.* **2024**, *13*, 440–445.

[7] a) S. Ito, T. Kato, K. Shinpo, K. Fujita, *Biochem. J.* **1984**, *222*, 407–411; b) T. J. Deming, *Curr. Opin. Chem. Biol.* **1999**, *3*, 100–105; c) J. H. Waiter, *Ann. N.Y. Acad. Sci.* **1999**, *875*, 301–309; d) H. Zhao, J. H. Waite, *Biochemistry* **2005**, *44*, 15915–15923; e) H. G. Silverman, F. F. Roberto, *Mar. Biotechnol.* **2007**, *9*, 661–681; f) B. K. Ahn, *J. Am. Chem. Soc.* **2017**, *139*, 10166–10171; g) S. Peplau, T. J. Neubert, K. Balasubramanian, J. Polleux, H. G. Börner, *Macromol. Rapid Commun.* **2023**, *44*, 2300300; h) A. Grafl, A. Müller, A. Preuß, B. Röder, H. G. Börner, *Adv. Eng. Mater.* **2023**, *25*, 2201279; i) S. Arias, S. Amini, J. M. Krüger, L. D. Bangert, H. G. Börner, *Soft Matter* **2021**, *17*, 2028–2033; j) N. L. Venkatareddy, P. Wilke, N. Ernst, J. Horsch, M. Weber, A. Dallmann, H. G. Börner, *Adv. Mater. Interfaces* **2019**, *6*, 1900501.

[8] H. Lee, N. F. Scherer, P. B. Messersmith, *Proc. Natl. Acad. Sci. U.S.A.* **2006**, *103*, 12999–13003.

[9] a) J. Yu, W. Wei, E. Danner, R. K. Ashley, J. N. Israelachvili, J. H. Waite, *Nat. Chem. Biol.* **2011**, *7*, 588–590; b) J. Yu, W. Wei, E. Danner, J. N. Israelachvili, J. H. Waite, *Adv. Mater.* **2011**, *23*, 2362–2366.

[10] a) M. S. Akram Bhuiyan, J. D. Roland, B. Liu, M. Reaume, Z. Zhang, J. D. Kelley, B. P. Lee, *J. Am. Chem. Soc.* **2020**, *142*, 4631–4638; b) M. S. A. Bhuiyan, B. Liu, J. Manuel, B. Zhao, B. P. Lee, *Biomacromolecules* **2021**, *22*, 4004–4015.

[11] a) B. D. B. Tiu, P. Delparastan, M. R. Ney, M. Gerst, P. B. Messersmith, *ACS Appl. Mater. Interfaces* **2019**, *11*, 28296–28306; b) B. D. B. Tiu, P. Delparastan, M. R. Ney, M. Gerst, P. B. Messersmith, *Angew. Chem. Int. Ed.* **2020**, *59*, 16616–16624; c) K. Lee, B. D. B. Tiu, V. Martchenko, K. Mai, G. Lee, M. Gerst, P. B. Messersmith, *ACS Appl. Mater. Interfaces* **2021**, *13*, 3161–3165; d) G. D. Degen, P. Delparastan, B. D. B. Tiu, P. B. Messersmith, *ACS Appl. Mater. Interfaces* **2022**, *14*, 6212–6220.

[12] a) L. Fischer, A. K. Strzelczyk, N. Wedler, C. Kropf, S. Schmidt, L. Hartmann, *Chem. Sci.* **2020**, *11*, 9919–9924; b) K. J. Winstanley, D. K. Smith, *J. Org. Chem.* **2007**, *72*, 2803–2815; c) J. J. Dannenberg, *J. Mol. Struct.* **2002**, *615*, 219–226; d) D. Rı bena, A. Alekseev, O. van Asselen, G. J. A. Mannie, M. M. R. M. Hendrix, L. G. J. van der Ven, N. A. J. M. Sommerdijk, G. de With, *Langmuir* **2012**, *28*, 16900–16908; e) C.-Y. Lin, J. C. Liu, *ACS Appl. Bio Mater.* **2020**, *3*, 3894–3905.

[13] a) S. Lamping, T. Otremba, B. J. Ravoo, *Angew. Chem. Int. Ed.* **2018**, *57*, 2474–2478; b) S. Lamping, B. J. Ravoo, *J. Mater. Chem. C* **2017**, *5*, 5882–5886; c) S. Lamping, L. Stricker, B. J. Ravoo, *Polym. Chem.* **2019**, *10*, 683–690; d) O. Roling, K. De Bruycker, B. Vonhören, L. Stricker, M. Körsgen, H. F. Arlinghaus, B. J. Ravoo, F. E. Du Prez, *Angew. Chem. Int. Ed.* **2015**, *54*, 13126–13129.

[14] M. Portigliatti, H. Hervet, L. Léger, *C. R. Acad. Sci., Ser. IV: Phys.* **2000**, *1*, 1187–1196.

[15] C. W. Paul, in *Handbook of Adhesion Technology* (Eds.: L. F. M. da Silva, A. Öchsner, R. D. Adams), Springer Berlin Heidelberg, Berlin, Heidelberg, **2011**, pp. 341–372.

[16] a) S. Okada, Y. Kashihara, T. Hirai, S. Fujii, Y. Nakamura, Y. Urahama, M. Ito, X. Liang, K. Nakajima, *J. Appl. Polym. Sci.* **2019**, *136*; b) K. Takahashi, R. Oda, K. Inaba, K. Kishimoto, *Soft Matter* **2020**, *16*, 6493–6500; c) K. Takahashi, F. Yanai, K. Inaba, K. Kishimoto, Y. Kozone, T. Sugizaki, *Langmuir* **2021**, *37*, 11457–11464.

[17] a) T. Takata, R. Tajima, W. Ando, *J. Org. Chem.* **1983**, *48*, 4764–4766; b) M. Cencer, Y. Liu, A. Winter, M. Murley, H. Meng, B. P. Lee, *Biomacromolecules* **2014**, *15*, 2861–2869; c) H. J. Meredith, C. L. Jenkins, J. J. Wilker, *Adv. Funct. Mater.* **2014**, *24*, 3259–3267.

[18] S. Arndt, D. Weis, K. Donsbach, S. R. Waldvogel, *Angew. Chem. Int. Ed.* **2020**, *59*, 8036–8041.

[19] K. Hinrichs, M. Gensch, N. Esser, *Appl. Spectrosc.* **2005**, *59*, 272A–282A.

[20] C. Leng, Y. Liu, C. Jenkins, H. Meredith, J. J. Wilker, Z. Chen, *Langmuir* **2013**, *29*, 6659–6664.

[21] M. Frigerio, M. Santagostino, S. Sputore, *J. Org. Chem.* **1999**, *64*, 4537–4538.

[22] J. B. Plumb, D. J. Harper, *Chem. Eng. News* **1990**, *68*, 3.

[23] A. Röseler, E.-H. Korte, in *Handbook of Vibrational Spectroscopy*, **2001**.
[24] K. Hinrichs, K.-J. Eichhorn, *Ellipsometry of Functional Organic Surfaces and Films*, 2nd ed., Springer, Cham, Switzerland **2018**.
[25] M. Wojdyr, *J. Appl. Crystallogr.* **2010**, *43*, 1126–1128.
[26] L. F. Gamon, J. M. White, U. Wille, *Org. Biomol. Chem.* **2014**, *12*, 8280–8287.
[27] B. M. Bizzarri, A. Martini, F. Serafini, D. Aversa, D. Piccinino, L. Botta, N. Berretta, E. Guatteo, R. Saladino, *RSC Adv.* **2017**, *7*, 20502–20509.
[28] S. H. Kim, T. Söhnel, J. Sperry, *Org. Lett.* **2020**, *22*, 3495–3498.
[29] S. Ito, G. Prota, *Experientia* **1977**, *33*, 1118–1119.
[30] JPK Instruments, in online brochure, Bruker Nano GmbH, https://www.jpk.com/app-technotes-img/AFM/pdf/jpk-tech-quantitative-imaging.14-1.pdf, **2021**.
[31] H. J. Butt, M. Jaschke, *Nanotechnology* **1995**, *6*, 1.
[32] J. E. Sader, J. W. M. Chon, P. Mulvaney, *Rev. Sci. Instrum.* **1999**, *70*, 3967–3969.
[33] D. C. Lin, E. K. Dimitriadis, F. Horkay, *J. Biomech. Eng.* **2006**, *129*, 430–440.
[34] JPK_Instruments, in online brochure, Bruker Nano GmbH, https://www.bruker.com/en/products-and-solutions/microscopes/bioafm/resource-library/determining-the-elastic-modulus-of-biological-samples-using-the-atomic-force-microscope/ jcr content/root/sections/section/sectionpar/twocolumns/contentpar-2/calltoaction.download-asset.pdf/primaryButton/jpk-app-elastic-modulus.14-1.pdf.
[35] P. Louette, F. Bodino, J.-J. Pireaux, *Surf. Sci. Spectra* **2005**, *12*, 27–31.
[36] H. Wagreich, J. M. Nelson, *J. Biol. Chem.* **1936**, *115*, 459–465.
[37] G. P. Maier, C. M. Bernt, A. Butler, *Biomater. Sci.* **2018**, *6*, 332–339.
[38] R. Pinnataip, B. P. Lee, *ACS Omega* **2021**, *6*, 5113–5118.
[39] J. Wang, W. Guo, K. Tian, X. Li, X. Wang, P. Li, Y. Zhang, B. Zhang, B. Zhang, S. Liu, X. Li, Z. Xu, J. Xu, H. Wang, Y. Hou, *Nano-Micro Lett.* **2023**, *16*, 62.

Manuscript received: May 3, 2024
Revised manuscript received: June 12, 2024
Accepted manuscript online: July 27, 2024
Version of record online: September 17, 2024